Charge carrier dynamics in organic semiconductors and their donor-acceptor composites: Numerical modeling of time-resolved photocurrent

Brian Johnson, Mark J. Kendrick, and Oksana Ostroverkhova

Charge carrier dynamics in organic semiconductors and their donor-acceptor composites: Numerical modeling of time-resolved photocurrent

Brian Johnson, Mark J. Kendrick, and Oksana Ostroverkhova[a)]
Department of Physics, Oregon State University, Corvallis, Oregon 97331, USA

We present a model that describes nanosecond (ns) time-scale photocurrent dynamics in functionalized anthradithiophene (ADT) films and ADT-based donor-acceptor (D/A) composites. By fitting numerically simulated photocurrents to experimental data, we quantify contributions of multiple pathways of charge carrier photogeneration to the photocurrent, as well as extract parameters that characterize charge transport (CT) in organic films including charge carrier mobilities, trap densities, hole trap depth, and trapping and recombination rates. In pristine ADT films, simulations revealed two competing charge photogeneration pathways: fast, occurring on picosecond (ps) or sub-ps time scales with efficiencies below 10%, and slow, which proceeds at the time scale of tens of nanoseconds, with efficiencies of about 11%–12%, at the applied electric fields of 40–80 kV/cm. The relative contribution of these pathways to the photocurrent was electric field dependent, with the contribution of the fast process increasing with applied electric field. However, the total charge photogeneration efficiency was weakly electric field dependent exhibiting values of 14%–20% of the absorbed photons. The remaining 80%–86% of the photoexcitation did not contribute to charge carrier generation at these time scales. In ADT-based D/A composites with 2 wt.% acceptor concentration, an additional pathway of charge photogeneration that proceeds via CT exciton dissociation contributed to the total charge photogeneration. In the composite with the functionalized pentacene (Pn) acceptor, which exhibits strong exciplex emission from a tightly bound D/A CT exciton, the contribution of the CT state to charge generation was small, ∼8%–12% of the total number of photogenerated charge carriers, dependent on the electric field. In contrast, in the composite with PCBM acceptor, the CT state contributed about a half of all photogenerated charge carriers. In both D/A composites, the charge carrier mobilities were reduced and trap densities and average trap depths were increased, as compared to a pristine ADT donor film. A considerably slower recombination of free holes with trapped electrons was found in the composite with the PCBM acceptor, which led to slower decays of the transient photocurrent and considerably higher charge retention, as compared to a pristine ADT donor film and the composite with the functionalized Pn acceptor.
© 2013 AIP Publishing LLC. [http://dx.doi.org/10.1063/1.4820259]

I. INTRODUCTION

Organic donor-acceptor (D/A) composites are of interest for applications in solar cells,[1] lasers,[2] photodetectors,[3,4] and photorefractive devices[5] due to enhanced charge carrier photogeneration resulting from the photoinduced charge transfer (CT) between the donor (D) and acceptor (A) molecules. While currently most high-performance bulk heterojunctions (BHJs) are based on polymer/fullerene composites, performance of small-molecule BHJs (SMBHJs), which are still relatively unexplored, is rapidly improving,[6] with several SMBHJ-based solar cells exhibiting power conversion efficiencies of 6%–7%.[7,8] In order to further improve performance of BHJs, including SMBHJs, it is important to understand mechanisms of charge carrier photogeneration, transport, and recombination, as well as their contribution to the photocurrent, in both pristine organic semiconductor materials and their D/A composites. Many recent studies have addressed dynamics and propensity for dissociation of CT states,[9–19] effects of D/A LUMO and HOMO energy offsets,[20–24] and of D/A molecular packing at the D/A interfaces,[25] in polymer-based BHJs, whereas relatively few studies have explored similar issues in SMBHJs.[26–30] For SMBHJs, of particular interest are solution-processable photoconductive organic semiconductors with high charge carrier mobilities and solid-state packing favoring efficient charge separation at the D/A interfaces.[31] Examples of such materials are functionalized pentacene (Pn) and anthradithiophene (ADT) derivatives which exhibit thin-film charge carrier (hole) mobilities of above ∼1.5 cm^2/(Vs), fast photoresponse, high photoconductivity under continuous wave (cw) excitation,[32–34] and a variety of solid-state packing motifs controlled by functionalization of the molecules.[35] Investigation of mechanisms of charge photogeneration and transport in such materials and their D/A composites is the focus of this paper.

One of the difficulties in establishing physical mechanisms of photoexcited charge carrier dynamics in organic

---

[a)]Electronic mail: oksana@science.oregonstate.edu

films is that experimentally measured photocurrents include contributions of a variety of processes that are challenging to disentangle, so that several different experimental techniques need to be applied to the same film in order to study each process separately. Numerical modeling of the photocurrent dynamics may provide a valuable insight into the relative contribution of each process to the photocurrent, thus avoiding multiple experiments. A considerable amount of such work has been done in polymer-based films, including Monte Carlo simulations of hopping conduction of photoexcited carriers,[36–38] numerical modeling of the time-resolved photocurrent dynamics on various time scales,[39–41] and modeling of the photocurrent in solar cells.[36,42–46]

In this paper, we present numerical modeling of nanosecond (ns) time-scale time-resolved photocurrent dynamics in ADT films and ADT-based D/A composites. For our studies, we chose a fluorinated ADT derivative functionalized with triethylsilylethynyl (TES) side groups, ADT-TES-F, as the donor and either PCBM or a fluorinated Pn derivative (Pn-TIPS-F8) functionalized with triisopropylsilylethynyl (TIPS) side group as acceptors (Fig. 1).[27] The choice of these particular systems for numerical simulations was motivated by our extensive previous experimental work with these materials, which enabled us to check results of the numerical modeling against various experimentally observed trends in time-resolved photoluminescence (PL), photoconductivity, and charge carrier mobility.[27,33,47,48] We quantified contributions of multiple pathways of charge photogeneration to ns time-scale photocurrent which include fast formation of spatially separated charge carriers, slow charge carrier photogeneration via Frenkel exciton (FE) dissociation, and in D/A composites, charge photogeneration via CT exciton dissociation. Additionally, we obtained parameters pertaining to subsequent transport of photoexcited charge carriers such as charge carrier mobilities, charge trapping, and recombination properties.[27,47]

II. EXPERIMENTAL

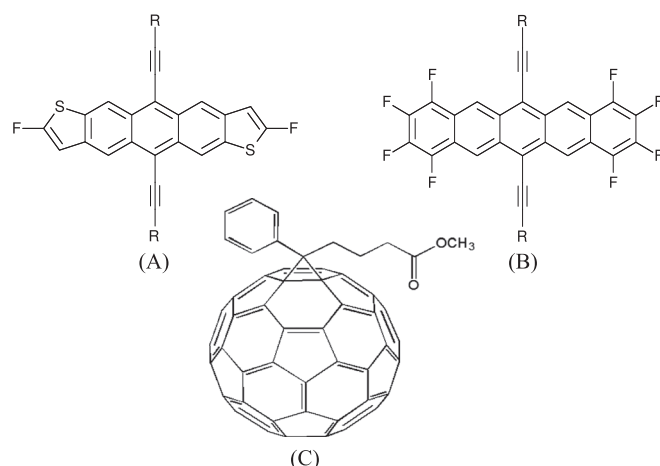Details of sample preparation and experimental set up used in measurements of ns time-scale time-resolved

FIG. 1. Molecular structures of the materials used in our study. (a) ADT-R-F, R = TES; (b) Pn-R-F8, R = TIPS; (c) PCBM.

photocurrent can be found in a previous paper.[27] Briefly, either pristine ADT-TES-F films or composite films containing 98 wt. % of ADT-TES-F donor and 2 wt.% of acceptor molecules were drop cast from toluene solutions onto glass substrates patterned with interdigitated Cr/Au electrodes with a $L = 25\,\mu m$ gap between the electrodes.[27] This method yielded polycrystalline films, as confirmed by x-ray diffraction. The HOMO (LUMO) energies were 5.35 (3.05) eV for ADT-TES-F, 5.55 (3.6) eV for Pn-TIPS-F8, and 6.1 (3.7) eV for PCBM. The low concentration of acceptor molecules in the D/A composites was chosen to minimize the disruption of film crystallinity and focus on processes at and due to heterojunctions, while neglecting effects of acceptor aggregation and acceptor domain formation. Voltage was applied to the samples, and dark current was measured as a function of voltage using a Keithley 237 source-measure unit. The average applied electric field E was calculated as $E = V/L$, and the studied range of electric fields was 20–80 kV/cm. For the transient photocurrent measurements, the samples were excited with a 355 nm ($\sim$3.49 eV), 0.18 $\mu J/cm^2$, 500 ps pulsed laser beam (cavity Q-switched frequency-tripled Nd:YAG laser, 44.6 kHz, from Nanolase, Inc.). The transient photocurrent was measured using a 50 GHz digital sampling oscilloscope (DSO) (CSA8200/Tek80E01) with a broadband amplifier (Centellax UAOL65VM). The time resolution of the system was $\sim$0.6 ns, limited by the laser pulse width and jitter. For comparison with simulated currents, both dark current and transient photocurrent values were converted to corresponding current densities, assuming an active transport channel depth of $d = 1\,\mu m$, based on an average thickness of our films.

III. THEORY

A considerable recent effort was directed towards numerical modeling of the photocurrent in organic solar cells.[49] Most approaches have focused either on solving a fully space-dependent set of drift-diffusion equations[42,50–53] or on Monte Carlo simulations of photoexcited charge carriers.[36–38] For our device geometry, a system of drift-diffusion equations is excessively computationally expensive to solve, since the channel length of the device is 25 μm, more than two orders of magnitude larger than that in typical solar cells. Instead, we assumed that the electric field and carrier densities can be averaged to a uniform spatial distribution and that under our experimental conditions drift current dominates over diffusion. The former assumption is supported by our previous observation of weak dependence of the amplitudes and dynamics of fast transient photocurrents on the position of the localized excitation in the gap between the electrodes.[33] The latter consideration is similar to that applied to modeling cw photocurrent dynamics in, for example, photorefractive polymer devices,[40,41] and to modeling transient photocurrent decays[39] in polymeric devices with channel lengths on the order of tens of microns.

A. Charge photogeneration

Our previous studies of pristine ADT films revealed fast charge carrier photogeneration (inferred from sub-30 ps

photocurrent rise times under 100 fs pulsed excitation, limited by the time resolution of the DSO detection), high cw photoconductivity, and relatively strong PL,[33,54,55] which indicates existence of several relaxation pathways following the photoexcitation. In particular, fast charge carrier photogeneration observed upon excitation of films with a pulsed light with a photon energy considerably above the ADT-TES-F HOMO-LUMO gap of 2.3 eV (such as with a 3.49 eV light used here) could be due to a direct band-to-band excitation of charge carriers[26] or due to hot exciton dissociation at ps or sub-ps time scales.[56,57] Regardless of the exact origin of the carriers created on fast (ps or sub-ps) time scales, in our further discussion, we will refer to such carriers as "spatially separated carriers" (SCC) (charge generation path 1 in Fig. 2). Additionally, a large percentage of the initial excitation relaxes into a FE which could dissociate under applied electric fields creating charge carriers contributing to the photocurrent at time scales of the exciton lifetime (path 2 in Fig. 2). In the D/A composite films, our previous work[27,47,58] suggests the existence of yet additional channel of charge carrier photogeneration due to dissociation of the CT exciton created by a Coulombically bound hole on the donor molecule and an electron on the acceptor molecule (path 4 in Fig. 2). Efficiency of this channel depends on the properties of the CT state dictated by the offset of LUMO energies of the donor and acceptor and by the D/A separation at the D/A interface.[27] In both pristine ADT-TES-F films and D/A composites, there are also relaxation pathways that do not contribute to charge carrier photogeneration (path 3 in Fig. 2), such as tightly bound excitons recombining to the ground state with or without PL emission.

B. Charge transport

The concentration of acceptor molecules in our D/A composites is sufficiently low for the acceptor domain formation to be neglected, so that an effective medium approach can be used, with charge carrier mobilities μ_n and μ_p representing the transport of electrons and holes, respectively, through the ADT-TES-F donor modified by the presence of
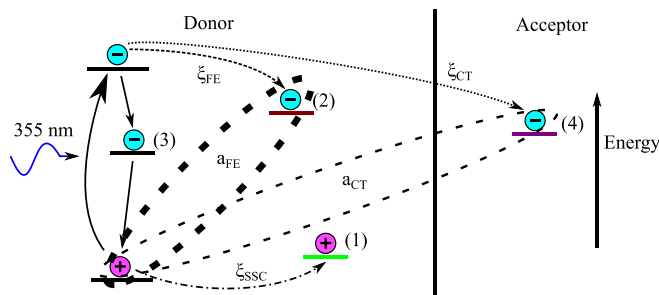

FIG. 2. Schematic of the different relaxation pathways upon photoexcitation, with pathways 1, 2, and 4 leading to charge generation described by the model of Eqs. (1)–(12). (1) Fast formation of SSC; (2) Formation of a FE in ADT-TES-F, which can dissociate at ns time-scales to free charge carriers; (3) Formation of a relaxed exciton that does not yield free charge carriers at ns time-scales and instead recombines to the ground state either radiatively or non-radiatively; (4) CT exciton in D/A composites that can dissociate to free carriers during its lifetime. Parameters $\xi_{SSC,FE,CT}$ represent fractions of the absorbed photon density corresponding to the SSC, FE, or CT pathways, and $a_{FE,CT}$ is an electron-pair separation in the FE or CT exciton.

acceptor molecules. In keeping with our previous studies of temperature dependent photocurrents in ADT-TES-F films and their D/A composites, we consider a Poole-Frenkel electric field dependence for these mobilities.[58] Charge carrier trapping effects are incorporated in the model via trapping parameters B_p (B_n) for holes (electrons) and total available hole (electron) trap densities of N_p (N_n). In ADT-TES-F films, holes are the majority carrier and are assumed to encounter shallower traps than electrons. Thus, in modeling photocurrent dynamics at ns time scales, we only include a charge detrapping effect for holes. To describe charge trapping and detrapping processes, we use the Miller-Abrahams model[37] such that the detrapping rate $B_{p_t} = \nu \times \exp[-\Delta/k_B T]$, where ν is the attempt-to-jump frequency, Δ is an average trap depth, T is the temperature (taken to be 300 K), and k_B is Boltzmann's constant. We further assume that for the non-thermally activated trapping process considered in the Miller-Abrahams model, ν is approximately equal to the product of the hole trapping parameter B_p and the hole trap density N_p. Also included in the model are bimolecular recombination with a rate γ and recombination of a free hole (electron) with a trapped electron (hole) with a rate $B_{p_f n_t}$ ($B_{n_f p_t}$).

C. Model

Given the considerations above, the resultant equations are as follows:

$$\frac{dn_f}{dt} = \xi_{SSC}(E)G(t) + k_{diss,FE}X_{FE} - \gamma n_f p_f$$
$$- B_n(N_n - n_t)n_f - B_{n_f p_t}n_f p_t$$
$$[+ k_{diss,CT}X_{CT}], \tag{1}$$

$$\frac{dn_t}{dt} = B_n(N_n - n_t)n_f - B_{p_f n_t}p_f n_t, \tag{2}$$

$$\frac{dp_f}{dt} = \xi_{SSC}(E)G(t) + k_{diss,FE}X_{FE} + B_{p_t}p_t - \gamma n_f p_f$$
$$- B_p(N_p - p_t)p_f - B_{p_f n_t}p_f n_t$$
$$[+ k_{diss,CT}X_{CT}], \tag{3}$$

$$\frac{dp_t}{dt} = B_p(N_p - p_t)p_f - B_{n_f p_t}n_f p_t - B_{p_t}p_t, \tag{4}$$

$$\frac{dX_{FE(CT)}}{dt} = \xi_{FE(CT)}(E)G(t) - k_{diss,FE(CT)}X_{FE(CT)}$$
$$- k_{r,FE(CT)}X_{FE(CT)}, \tag{5}$$

$$\gamma = e(\mu_n + \mu_p)/(\epsilon_0 \epsilon_r), \tag{6}$$

$$k_{diss,FE(CT)}(E,T) = \frac{3\gamma J_1(2\sqrt{-2b})}{4\pi a_{FE(CT)}^3 \sqrt{-2b}}\exp\left(-\frac{E_{B,FE(CT)}}{k_B T}\right), \tag{7}$$

$$b = (e^3|E|)/\left(8\pi\epsilon_0\epsilon_r(k_B T)^2\right), \tag{8}$$

$$J = eE\left(\mu_n(E)n_f + \mu_p(E)p_f\right), \tag{9}$$

$$\mu_{n(p)}(E) = \mu_{n0(p0)}\exp\left(\gamma_{n(p)}\sqrt{E}\right), \tag{10}$$

where t is the time, e is the fundamental charge, ϵ_0 is the permittivity of free space, and ϵ_r is the relative permittivity of the film (taken to be 3). Variables $p(n)_f$ correspond to free hole (electron) density, $p(n)_t$ is the trapped hole (electron) density, X_{FE} (X_{CT}) are exciton densities for the FE (CT exciton), J is the total current density, E is applied electric field, $G(t)$ is the photoexcitation rate described below (Eq. (12)), and $\xi_{SSC(FE)(CT)}$ are fractions of the photoexcitation that result in charge photogeneration via the SSC pathway and in the FE and CT exciton formation (pathways 1, 2, and 4, respectively, in Fig. 2). $k_{diss,FE}$ ($k_{diss,CT}$) are dissociation rates for the FE (CT exciton), and $k_{r,FE}$ ($k_{r,CT}$) are recombination rates for the FE (CT exciton). $E_{B,FE}$ ($E_{B,CT}$) is the binding energy of the FE (CT exciton) given by $E_{B,FE(CT)} = e^2/(4\pi\epsilon_0\epsilon_r a_{FE(CT)})$, where a_{FE} (a_{CT}) is the initial separation between charge carriers for the FE (CT exciton). Equations (1) and (3) are the coupled drift equations for hole and electron densities, with multiple charge generation paths as described above, charge trapping, and recombination including bimolecular recombination of free carriers to the ground state with the Langevin rate constant of Eq. (6). Bimolecular recombination with a formation of the FE or CT exciton was also considered,[53] but produced a negligible effect on the photocurrent dynamics and was omitted. Equations (2) and (4) describe the trapping, trap assisted recombination, and hole detrapping of carriers, governed by their respective rates. Equation (5) describes the dynamics of the dissociation and recombination of FEs and, in D/A composites, CT excitons. The dissociation rate of both FEs and CT excitons is given by Eq. (7), following the Onsager-Braun formalism.[59] μ_{p0} (μ_{n0}) and γ_p (γ_n) are Poole-Frenkel model parameters characterizing zero-field mobility and electric field dependence of mobility for holes (electrons).

Commonly used models of exciton dissociation, such as the Onsager-Braun model, consider the rate of dissociation k_{diss} electric field dependent, whereas the primary yield of geminate pair formation (ξ_{FE}) is typically assumed to be electric field independent; this assumption has been challenged in several studies.[60–62] We found that our data are more consistent with an electric field-dependent competition among pathways 1, 2, and, in composites, 4 of charge carrier photogeneration, which suggests field dependent parameters ξ_{SSC}, ξ_{FE}, and ξ_{CT}. Since the analytical function describing such competition is not known, in order to extract quantitative information about relative contributions of these different charge generation pathways to the photocurrent at various applied electric fields, we used the simplest possible linear model for the electric field dependence of these parameters, specifically

$$\xi_{SSC(FE)(CT)} = \xi_{SSC(FE)(CT)}^{(0)} + \gamma_{SSC(FE)(CT)}E, \quad (11)$$

where the parameters $\xi_{SSC(FE)(CT)}^{(0)}$ and $\gamma_{SSC(FE)(CT)}$ were taken to be constant over our range of electric fields. We found that this assumption worked well for pristine ADT-TES-F and ADT-TES-F/Pn-TIPS-F8 films up to electric fields of at least 80 kV/cm; however, in ADT-TES-F/PCBM films, the assumption started to break down at about 60 kV/cm (Sec. IV B).

The illumination profile of our films on interdigitated electrodes is taken to be uniform over the device. We calculated the generation rate $G(t)$ by first assuming a perfect Gaussian laser pulse with a full width at half maximum (FWHM) of $\tau = 500$ ps, representative of the laser pulse used in our experiments, and then multiplying it by the density of absorbed photons N_{ph}, which in our experiments is 2.9×10^{15} cm^{-3}. In particular,

$$G(t) = N_{ph}\frac{2\sqrt{\ln 2}}{\tau\sqrt{\pi}} * \exp\left(-4\ln 2\frac{(t - t_{FWTM}/2)^2}{\tau^2}\right), \quad (12)$$

where t_{FWTM} is the full width at a tenth of the maximum of the Gaussian pulse and so $G(t=0) = 0.1G_{max}$, where G_{max} is the photon density at the laser pulse maximum. The constants ensure that the pulse is normalized such that $\int_{-\infty}^{\infty} G(t)dt = N_{ph}$. For computational purposes, the infinite integration limits were replaced by those that correspond to the duration of the simulated transient photocurrent, 0 to 20 ns.

Based on non-negligible dark currents in our films, due mostly to efficient hole injection from Au electrodes,[33,55] we assumed that before the photoexcitation of the film there exists a certain density of free and trapped charge carriers that cannot be neglected.[63] We extracted average carrier densities[64] from dark current values as described in detail in the supplemental material,[65] and used them as initial conditions for corresponding densities in our simulations of transient photocurrents. Briefly, for boundary conditions, we have assumed thermionic injection[66,67] with image charge effects. The injection barriers for holes and electrons, ϕ_B^p and ϕ_B^n, respectively, were taken to be 0.25 eV and 2.05 eV, calculated from the HOMO and LUMO levels of ADT-TES-F and the work function of Au (5.1 eV). We then assumed that before the laser pulse excitation, the carrier densities have reached a steady state, so that $dp(n)/dt = 0$. Additionally, the density of chargeable sites in the material is considered to be identical for electrons and holes. Under these assumptions, we obtained[66] the following average densities at time $t = 0$:

$$n_f^0 = \frac{J_{Dark}(E)}{eE}\frac{e^{-\frac{\phi_B^n}{k_BT}}}{\mu_n e^{-\frac{\phi_B^n}{k_BT}} + \mu_p e^{-\frac{\phi_B^p}{k_BT}}}, \quad (13)$$

$$p_f^0 = \frac{J_{Dark}(E)}{eE}\frac{e^{-\frac{\phi_B^p}{k_BT}}}{\mu_n e^{-\frac{\phi_B^n}{k_BT}} + \mu_p e^{-\frac{\phi_B^p}{k_BT}}}, \quad (14)$$

$$n_t^0 = (B_n N_n n_f^0)/(B_n n_f^0 + B_{p_f n_t} p_f^0), \quad (15)$$

$$p_t^0 = (B_p N_p p_f^0)/(B_p p_f^0 + B_{n_f p_t} n_f^0 + B_{p_t}), \quad (16)$$

where $J_{Dark}(E)$ is the measured dark current density at the applied electric field E.

The system of Eqs. (1)–(12) with initial conditions given by Eqs. (13)–(16) was solved numerically in MATLAB using the built in ode15s function. The simulated transients were then fit to the data using the non-linear optimization package NLOPT.[68] Details of the fitting procedure, as well

as bounds used for each parameter and their justification, can be found in the supplemental material.[65] Briefly, the ISRES[69] algorithm was used for gross global fitting across a large initial parameter space, and the COBYLA[70] algorithm was used to perform fine local minimization. Both algorithms work by minimizing a user provided objective function. The objective functions used were

$$f_1(\vec{x}) = \sum_n \left(J_{Data}(t_n) - J_{Sim}(t_n, \vec{x})\right)^2, \quad (17)$$

$$f_2(\vec{x}) = \sum_m (1 - r_m^2), \quad (18)$$

where $\vec{x}$ is the vector input to the simulation function that incorporates all varied parameters of the model, t_n is the nth discrete time value, $J_{Data}(t_n)$ is the experimentally measured total current at t_n, $J_{Sim}(t_n, \vec{x})$ is the simulated total current at t_n, and r_m^2 is the coefficient of determination of the simulated fit for the mth applied electric field. Using these objective functions, we obtained sets of parameters that describe experimentally measured photocurrent transients at all applied electric fields in the studied range.

IV. RESULTS

We now describe the process of arriving at the compound model of Eqs. (1)–(5) used in simulating photocurrent transients in pristine ADT-TES-F films and ADT-TES-F-based D/A composites.

A. Pristine ADT-TES-F films

In modelling transient photocurrents in pristine ADT-TES-F films, we first considered a model which included only the fast SSC generation, pathway 1 in Fig. 2 ($Xi_{FE} = 0$ in Eqs. (1) and (3)). An example of the best fit result for the data taken at an applied electric field of 60 kV/cm is shown as the dashed line in the inset of Fig. 3(a). The simulated transient exhibited a fast rise followed by a considerably faster initial decay than the experimental data, with no additional, slow decay component. Although this model could reproduce the fast rise and initial decay at higher applied electric fields (above 60 kV/cm), it was unable to attain good fits for the data obtained at lower applied electric fields.

The next model examined was a model that only included the charge generation pathway via FE dissociation, pathway 2 in Fig. 2 ($\xi_{SSC} = 0$ in Eqs. (1) and (3)), and attempted to fit one of the experimental data sets using the objective function of Eq. (17). A sample of the best fit attained in this case for the data taken at an applied electric field of 60 kV/cm is shown in the inset to Fig. 3(a) as the dashed-dotted line. The fits revealed that the FE dissociation-only model showed a much slower photocurrent rise than the data and did not reproduce well the transition between the fast initial decay and slow decay component occurring at about 2–3 ns. This model was capable of generating better fits at lower electric fields, but the goodness-of-fit values r^2 of such fits were still relatively low, below 0.8.

Next, we combined the fast SSC generation (pathway 1) and charge generation via FE dissociation (pathway 2) into
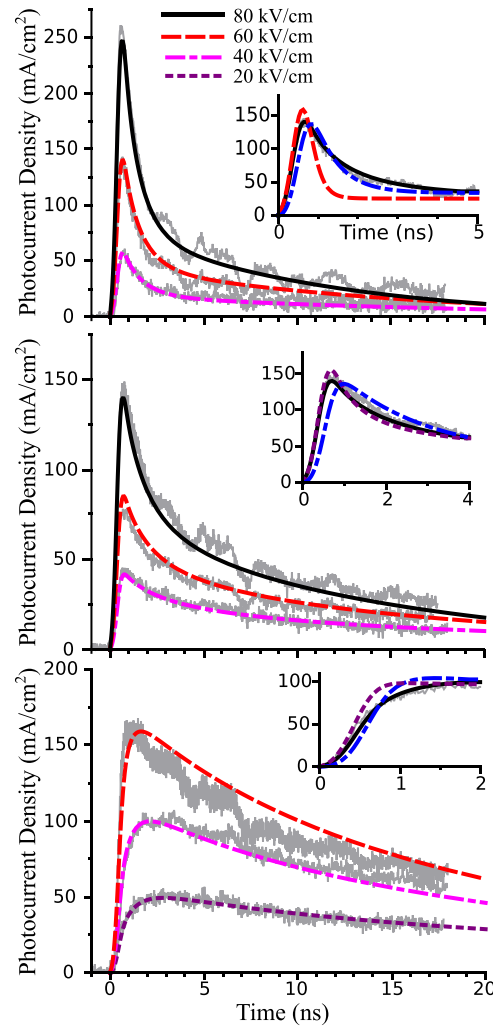

FIG. 3. Photocurrent densities, experimentally measured at various applied electric fields, superimposed with those simulated using Eqs. (1)–(12) with the parameters listed in Table I, for: (a) pristine ADT-TES-F film, (b) ADT-TES-F/Pn-TIPS-F8 2 wt. % composite, and (c) ADT-TES-F/PCBM 2 wt. % composite. Insets illustrate effects of different charge generation pathway choices and show best fits to the data obtained using: (a) at 60 kV/cm, SSC generation pathway 1 only (dashed line), FE dissociation pathway 2 only (dashed-dotted line), both pathways (solid line); (b) at 60 kV/cm and (c) at 40 kV/cm: FE dissociation pathway 2 only (dashed-dotted line), combined SSC and FE dissociation pathways 1 and 2, respectively (dashed line), and combined SSC, FE dissociation, and CT exciton dissociation pathways 1, 2, and 4, respectively (solid line).

one model. The results are presented in Fig. 3(a), with the short time-scale dynamics shown in more detail in the inset. The combined model displays the best aspects of SSC-only and FE dissociation-only models, with fast photocurrent rise, a moderately fast initial decay, and a slow decay component. This model provided consistent results for the data across the entire range of applied electric fields and attained goodness-of-fit values r^2 of 0.89–0.97 depending on the electric field.

Having found a model that could fit data at any single value of the applied electric field well, we generalized the fitting algorithm to fit data taken at all values of applied electric field simultaneously. In order to weight data for all of the different applied electric fields identically, we used Eq. (18) as the objective function. The fractions of absorbed photon density that resulted in the SSC (ξ_{SSC}) and in the formation
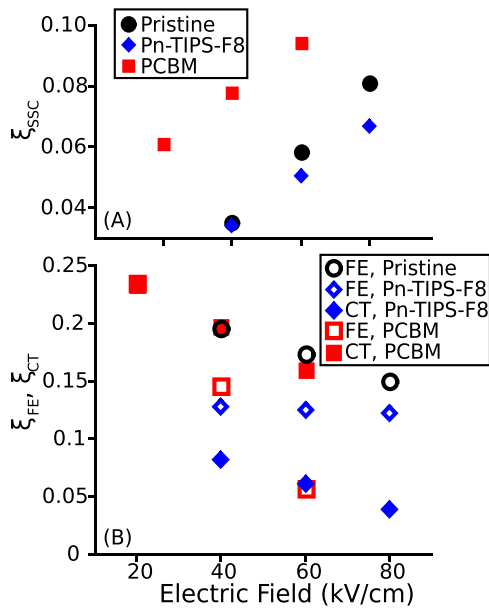
FIG. 4. Fractions of the absorbed photon density that result in photogenerated charge carriers via the SSC pathway 1 (a) and form FE and CT excitons (b) in a pristine ADT-TES-F film and ADT-TES-F/Pn-TIPS-F8 and ADT-TES-F/PCBM 2 wt.% D/A composites.

of the FE state (ξ_{FE}), as revealed by simulations (Fig. 3(a)), are shown in Figs. 4(a) and 4(b), respectively, at various applied electric fields. As the electric field increased from 40 kV/cm to 80 kV/cm, ξ_{SSC} increased from 0.035 to 0.081, whereas ξ_{FE} decreased from ~0.2 to 0.15. Good fits were obtained by applying the constraint $\gamma_{SSC} = -\gamma_{FE}$ to Eq. (11), suggesting that the pathways 1 and 2 are in direct competition with each other, originating from the same photoexcited state, such as a hot exciton. The FE dissociates with the electric field-dependent dissociation rate $k_{diss,FE}$ (Fig. 5) during its lifetime given by $1/(k_{diss,FE} + k_{r,FE})$ (Figs. 6 and S1). The efficiency of the exciton dissociation occurring over time scales of the exciton lifetime is given by

$$\eta_{FE(CT)} = \frac{k_{diss,FE(CT)}}{k_{diss,FE(CT)} + k_{r,FE(CT)}}. \quad (19)$$

For the FE in pristine ADT-TES-F films, η_{FE} varies between 0.56 and 0.77 in the studied range of electric fields. This yields the fraction of absorbed photon density which contributes to the photocurrent via the FE dissociation, $\xi_{FE}\eta_{FE}$, of
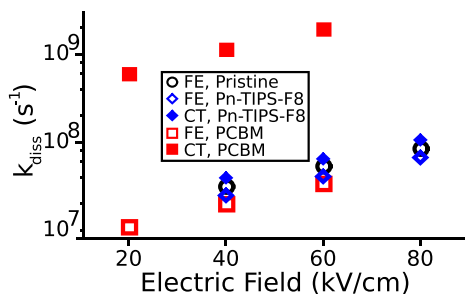

FIG. 5. Exciton dissociation rate for FE and CT excitons as a function of electric field for a pristine ADT-TES-F film and ADT-TES-F/Pn-TIPS-F8 and ADT-TES-F/PCBM 2 wt.% composites.
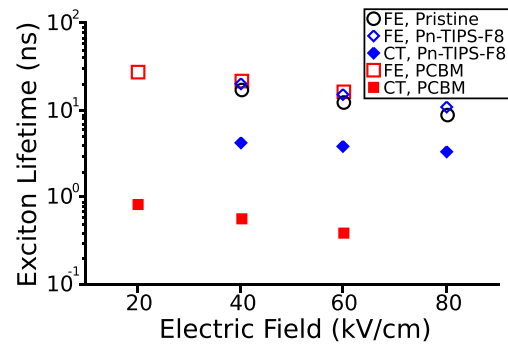

FIG. 6. FE and CT exciton lifetimes at various electric fields for a pristine ADT-TES-F film and ADT-TES-F/Pn-TIPS-F8 and ADT-TES-F/PCBM 2 wt.% composites.

~0.11 − 0.12, approximately same for all electric fields. The total efficiency of charge photogeneration, combined from pathways 1 and 2, on the time scales of the simulated transients of ~20 ns, is

$$\eta_{tot} = \xi_{SSC} + \xi_{FE}\eta_{FE}. \quad (20)$$

It increases from 0.14 to 0.20 upon an increase in the electric field from 40 kV/cm to 80 kV/cm, as shown in Fig. 7. The rest of the photoexcitation, given by $1 - \eta_{tot}$, which amounts to about 80%–86% of the absorbed photon density, depending on the applied electric field, does not contribute to charge carrier photogeneration in the time domain studied.

Table I lists values obtained from fits to experimental data for other parameters of Eqs. (1)–(12). Hole mobility, exhibiting a zero-field value of ~0.6 cm^2/(V s), is consistent with TFT and space-charge-limited current mobilities in similar films.[33,71] Hole trapping and detrapping properties seem to be well described by the Miller-Abrahams model, with the attempt-to-jump rate ν of 3.9×10^{10} s^{-1}, comparable to that in pentacene films,[72] and the average trap depth of 29 meV similar to that of 25 meV obtained from Arrhenius fits of experimentally measured temperature dependence of the transient photocurrent in ADT-TES-F films in a previous paper[58] by our group. The zero-field electron mobility was lower than the hole mobility[73] by a factor of ~6, whereas the average electron trap density was higher than the hole trap density by a factor of ~2.5 (Table I). Both hole and electron trap densities were on the order of 10^{18} cm^{-3}, similar to values reported by other groups[74] for small-molecule organic semiconductor films.
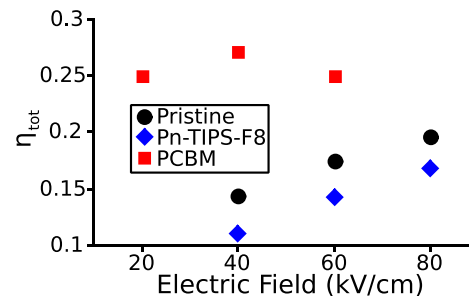

FIG. 7. Total charge generation efficiency as a function of electric field for a pristine ADT-TES-F film and ADT-TES-F/Pn-TIPS-F8 and ADT-TES-F/PCBM 2 wt.% composites.

TABLE I. Parameter values extracted from experimental data for pristine ADT-TES-F films and ADT-TES-F-based D/A composites with Pn-TIPS-F8 and PCBM acceptors using simulation with a system of Eqs. (1)–(12). Parameter descriptions are given in the text.

Parameter (unit)	ADT-TES-F	2% Pn-TIPS-F8	2% PCBM
$\mu_{n,0}$ $(\mathrm{cm^2(V\,s)^{-1}})$	0.093	0.016	0.025
$\mu_{p,0}$ $(\mathrm{cm^2(V\,s)^{-1}})$	0.60	0.51	0.36
γ_n $(\mathrm{cm/V})^{1/2}$	1.8×10^{-3}	2.0×10^{-3}	3.8×10^{-3}
γ_p $(\mathrm{cm/V})^{1/2}$	3.1×10^{-4}	6.0×10^{-4}	9.1×10^{-4}
Δ (meV)	29	41	39
N_n $(\mathrm{cm^{-3}})$	7.1×10^{18}	7.4×10^{18}	8.7×10^{19}
N_p $(\mathrm{cm^{-3}})$	2.8×10^{18}	2.2×10^{18}	3.8×10^{18}
$B_n N_n$ $(\mathrm{s^{-1}})$	5.1×10^{11}	8.9×10^{11}	7.8×10^{11}
$B_p N_p$ $(\mathrm{s^{-1}})$	3.9×10^{10}	6.9×10^{10}	2.1×10^{11}
$B_{n_f p_t}$ $(\mathrm{cm^3 s^{-1}})$	1.4×10^{-3}	5.0×10^{-3}	4.0×10^{-3}
$B_{p_f n_t}$ $(\mathrm{cm^3 s^{-1}})$	2.1×10^{-5}	2.7×10^{-5}	8.2×10^{-7}
a_{FE} (nm)	1.18	1.18	1.18
a_{CT} (nm)	…	1.22	1.77

B. D/A composites

The model that takes into account the SSC and FE channels of carrier photogeneration produced good fits for the pristine ADT-TES-F film photocurrents, but it was unable to accurately replicate some of the more complicated dynamics of photocurrents from composites. The insets of Figs. 3(b) and 3(c) show the best results of fitting the photocurrent at the electric fields of 60 kV/cm and 40 kV/cm in the ADT-TES-F/Pn-TIPS-F8 and ADT-TES-F/PCBM composites, respectively, with the models that include FE dissociation-only (dashed-dotted line, pathway 2 in Fig. 2) and both the SSC and FE dissociation pathways (dashed line, pathways 1 and 2, respectively, in Fig. 2). In addition, there was little consistency in the fits across the studied electric field range, and our multiple-electric-field fitting process was unable to replicate the correct electric field dependence of the transients. Our previous work[27] identified a possibility of charge generation via CT exciton dissociation in several D/A composites with the ADT-TES-F donor, with a CT exciton that may or may not be detectable by PL measurements, depending on the acceptor. For example, in the ADT-TES-F/Pn-TIPS-F8 D/A composite, an exciplex that formed between the donor HOMO and the acceptor LUMO was detected by the PL emission and was considered as a potential contributor of charge carriers via exciplex dissociation. In contrast, in the ADT-TES-F/PCBM D/A composite, no exciplex emission was detected; however, based on the photocurrent dynamics and partial quenching of the ADT-TES-F donor PL, it was inferred that there might exist dark CT states that form between the ADT-TES-F donor and PCBM acceptor, which could contribute to charge carrier generation.

Based on these considerations, to accurately reproduce the photocurrent dynamics in the composites with the Pn-TIPS-F8 and PCBM acceptors, we added the charge generation pathway 4 in Fig. 2, which proceeds via CT exciton dissociation, to the set of equations (Eq. (5)) and additional

terms to Eqs. (1) and (3). To describe CT exciton dissociation, we used the Onsager-Braun model, similar to that of the FE dissociation, but with a different initial pair separation a_{CT} and recombination rate $k_{r,CT}$. Thus, in D/A composites, there are three competing channels of charge photogeneration: the fast SSC pathway, FE dissociation, and CT exciton dissociation (pathways 1, 2, and 4, respectively, in Fig. 2), with relative contribution of each pathway to the overall charge photogeneration being electric field dependent. Since the exact pathway of the CT state formation is unknown,[26,58] we did not impose restrictions on the relative values of γ_{SSC}, γ_{FE}, and γ_{CT} in Eq. (11). Following the same fitting process as described above, we fit the experimental data to the simulated photocurrent transients (Fig. 3). The addition of the CT exciton dissociation improved the goodness-of-fit ratings for the fits to the data from the composite films (Figs. 3(b) and 3(c)). The fit to the data from the composite with the PCBM acceptor at an applied electric field of 60 kV/cm was lower in quality than the fits to the data at lower electric fields due to breaking down of the assumption of Eq. (11) at higher electric fields. As in pristine ADT-TES-F films, in both D/A composites under consideration, the efficiency of fast carrier generation via the SSC pathway was below 10% (Fig. 4(a)).

In the composite with the Pn-TIPS-F8 acceptor, ~0.12 (~0.04–0.08) of the absorbed photon density N_{ph} formed the charge-generating FE (CT exciton) (Fig. 4(b)). These dissociated during their lifetimes (Figs. 6 and S1) with the electric field dependent efficiency η_{FE} (η_{CT}), calculated using Eq. (19), of 0.49–0.72 (0.17–0.35) in the studied range of electric fields. This yields a fraction of N_{ph} contributing to the overall charge photogeneration via the FE (CT exciton) dissociation pathway, $\xi_{FE}\eta_{FE}$ ($\xi_{CT}\eta_{CT}$), of 0.062–0.088 (0.014–0.015). The contribution of the CT dissociation to charge carrier generation in this composite, given by $\xi_{CT}\eta_{CT}/\eta_{tot}$, is the lowest of the three contributing pathways at 8%–12%, which is consistent with our previous observation of a strong PL emission from the ADT-TES-F/Pn-TIPS-F8 CT state (exciplex), indicative of a tightly bound CT state with a relatively low dissociation rate $k_{diss,CT}$ (Fig. 5).[27] The total fraction of the absorbed photon density which results in charge carrier photogeneration at time scales of ~20 ns, is

$$\eta_{tot} = \xi_{SSC} + \xi_{FE}\eta_{FE} + \xi_{CT}\eta_{CT}. \quad (21)$$

It increases slightly, from ~0.11 to ~0.17, as the electric field increases from 40 kV/cm to 80 kV/cm (Fig. 7). The rest of the photoexcitation, given by $1 - \eta_{tot}$, which amounts to ~83%–89% of the absorbed photons, does not contribute to charge carrier photogeneration in the time domain studied.

In the composite with the PCBM acceptor, the CT exciton formed considerably more efficiently (ξ_{CT} in Fig. 4(b)) and was considerably more prone to dissociation as compared to that in the composite with the Pn-TIPS-F8 acceptor. As a result, the contribution of the CT exciton dissociation (pathway 4) into the overall charge photogeneration, $\xi_{CT}\eta_{CT}$, of 0.12–0.13 (i.e., 12%–13%) of the absorbed photon density was a factor of ~8.5 larger than that in the ADT-TES-F/Pn-TIPS-F8 composite. It also dominated over the pathway 2

(charge generation via FE dissociation), especially at low electric fields, which converted $\xi_{FE}\eta_{FE} = 0.03 - 0.07$ (i.e., 3%–7%) of the absorbed photons into charge carriers.

Table I summarizes other parameters pertaining to charge generation and transport in the studied D/A composites. In both composites, the hole and electron mobilities were reduced as compared to those in pristine ADT-TES-F films, whereas the average trap densities were increased; this result is expected, given our effective medium approach to charge transport modeling in these composites with low acceptor concentration. In both composites, the effective hole trap depth was increased with respect to that in pristine ADT-TES-F films (41 and 39 meV in the composites with Pn-TIPS-F8 and PCBM, respectively), due to an increased disorder in the composite films.

V. DISCUSSION

Figure 8 summarizes the distribution of the photoexcitation among various pathways for the pristine ADT-TES-F films and ADT-TES-F/Pn-TIPS-F8 and ADT-TES-F/PCBM composites at low acceptor concentrations, obtained from simulations of the photocurrents over ~20 ns, at the applied electric field of 40 kV/cm. In pristine ADT-TES-F films at this field, the contribution of the pathway 2 (FE dissociation) to ns time-scales charge photogeneration was a factor of ~3.1 larger than that of the pathway 1. This dominance of the pathway 2 progressively reduced as the electric field increased. In ADT-TES-F/Pn-TIPS-F8 composites, the pathway 2 dominated over the pathway 1 by a factor of ~1.6, whereas the contribution of the pathway 4 (CT exciton dissociation) to the charge generation was a factor of ~4.5 lower than that of the pathway 2 and slightly decreased with the electric field. In contrast, in ADT-TES-F/PCBM composites, pathway 4 was the dominant factor, contributing about half of all charge carriers ($\xi_{CT}\eta_{CT}/\eta_{tot} \approx 0.49$), whereas the other half was distributed between the pathways 1 and 2. The pathway 4 contribution was weakly field dependent in the studied range, whereas the trends in relative contributions of the pathways 1 and 2 followed those of pristine ADT-TES-F films. Note that in spite of electric field dependence of various parameters contributing to charge photogeneration, the total charge photogeneration efficiency in ADT-TES-F/PCBM

composites (Fig. 7) is electric field independent in the studied range of electric fields, similar to that reported in D/A systems with polymeric donors and PCBM acceptors.[75,76]

Ultrafast charge carrier photogeneration has been observed in a variety of small-molecule and polymeric organic semiconductors via ultrafast spectroscopy methods,[26,77–79] Auston switch-based techniques,[39,80,81] and fast oscilloscope detection of photocurrents.[33,54,82] In most cases, the efficiency of this process is at or below ~10%, in agreement with values of ξ_{SSC} (which dominates charge generation at fast time scales) extracted from our simulations. Many of these methods enable determination of the product of the sum of hole and electron mobilities ($\mu_{tot} = \mu_p + \mu_n$) and of the photogeneration efficiency. In our films the $\mu_{tot}\xi_{SSC}$ values (Fig. 4(a) and Table I) are between ~0.02 and 0.06 cm^2/V s, in good agreement with experimental observations from similar films.[33,54,78] However, the mechanism of achieving the SSC state at ultrafast time scales in ADT films is unknown and requires further investigation. Two main possibilities are direct band-to-band excitations[26] and hot exciton dissociation,[56] with the electric field dependence of the parameter ξ_{SSC} observed here more consistent with the latter process.

The simulations revealed that a FE with lifetimes on the order of 10–20 ns (Figs. 6 and S1) contributes a considerable number of charge carriers at ns time-scales through pathway 2 in Fig. 2. In the studied D/A composites, the FE lifetimes were similar to those in the pristine ADT-TES-F film (Fig. 6), which confirms that the FE state is formed on the ADT-TES-F donor. There are several possible origins of such FE states. For example, these could be dark states that are delocalized over several ADT-TES-F molecules in the ADT-TES-F H-aggregates,[58] similar to those in H-aggregates of sexithiophene films.[83] The pristine ADT-TES-F films and both D/A composites considered here exhibit a relatively strong PL from the relaxed ADT-TES-F excitons.[27,58] The emissive ADT-TES-F excitons at room temperature are highly mobile within disordered ADT-TES-F H-aggregates, which shortens their PL lifetimes from about 13 ns (for isolated molecules) to 1–2 ns (in films).[58] Our previous work revealed that these excitons do not contribute to photocurrents at ns time-scales and cannot be the charge-generating FE states of Fig. 2.[27,58] Instead, these are the excitons that constitute most of the photoexcitation (~80% of absorbed photons) that does not
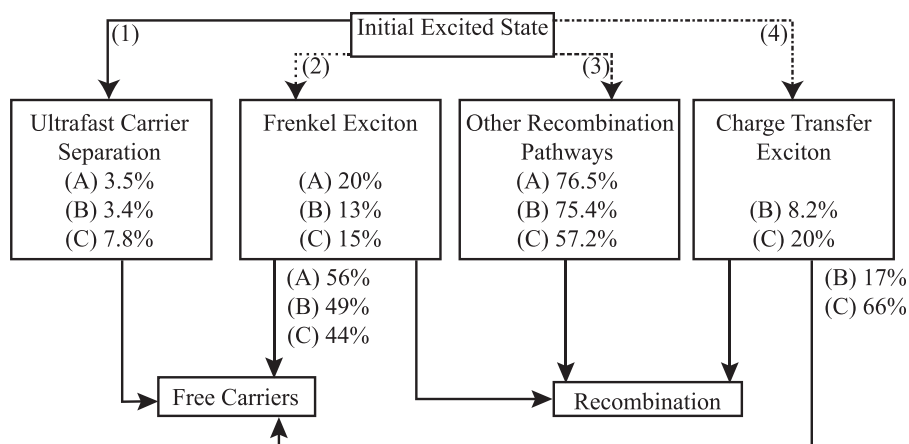

FIG. 8. Summary of distribution of the total photoexcitation (100%) among various relaxation paths at an applied electric field of 40 kV/cm. Values are given for a pristine ADT-TES-F film (A), an ADT-TES-F/Pn-TIPS-F8 2 wt. % composite film (B), and an ADT-TES-F/PCBM 2 wt.% composite film (C). Values in boxes are fractions ξ from Fig. 4 multiplied by 100%, whereas values below the boxes are dissociation efficiencies $\eta_{FE,CT}$ of Eq. (19), also multiplied by 100%.

produce charge carriers. However, since the PL lifetimes of the FE in Fig. 6 are close to PL lifetimes of isolated ADT-TES-F molecules,[33] the alternative assignment for the FE states observed here could be relatively immobile ADT-TES-F excitons, possibly formed at grain boundaries, which are longer lived and have more time to dissociate as compared to highly mobile excitons that constitute the majority of the photoexcited species.[58]

The simulations established that the CT state in the ADT-TES-F/Pn-TIPS-F8 composite, contributing to charge photogeneration through pathway 4 in Fig. 2, exhibits lifetimes of 3.4–4.5 ns (Fig. 6). These are close to experimentally measured PL lifetimes of the exciplex (3.8–4.6 ns, depending on the applied electric field) in this composite, which suggests that the nature of the charge-generating CT state in Fig. 2 is the exciplex whose properties we have reported previously.[27] Indeed, low contribution of the CT states to the photocurrent in this composite is consistent with a highly emissive tightly bound exciplex, in agreement with experiments.[27] The CT state in the composite with the PCBM acceptor was found to exhibit considerably lower lifetimes (Figs. 6 and S1) than those of the ADT-TES-F FE and the CT in the composite with the Pn-TIPS-F8 acceptor. Additionally, it was more dissociative than either of these excitons (Fig. 5), which is consistent with a larger LUMO offset between ADT-TES-F and PCBM and larger D/A separation due to the size of the PCBM molecule as compared to Pn-TIPS-F8, both of which factors have been shown to enhance the photocurrent.[27,84] Our simulations confirm the latter statement, yielding the initial charge pair separation a_{CT} of 1.77 nm in the ADT-TES-F/PCBM composite, as compared to that of 1.22 nm in the ADT-TES-F/Pn-TIPS-F8 composite.

The total amount of charge generated at ns time-scales, 0.1–0.25 of absorbed photon density (Fig. 7), only differs by a factor of ∼2 in all three systems under study, with the highest in the composite with the PCBM acceptor followed by pristine ADT-TES-F film and the composite with the Pn-TIPS-F8 acceptor, consistent with our previous observations.[27] However, our previous studies[27] also established that the amount of mobile charge over the period of 1 μs, obtained by integrating transient photocurrents over this time period, as well as photocurrents obtained under cw illumination, are considerably higher (by a factor of ∼6–10) in the composite with the PCBM acceptor as compared to pristine ADT-TES-F films. Based on our simulation results, this is due to a considerably lower rate of recombination between trapped electrons and free holes in the ADT-TES-F/PCBM composite ($B_{p_f n_t}$ in Table I and Fig. S2), which results in a significantly slower decay of the photocurrent in this composite, and thus, higher charge retention, as compared to that in pristine ADT-TES-F films.

VI. CONCLUSIONS

We presented a model based on drift conduction which enabled us to quantify contributions of multiple pathways to charge carrier photogeneration, as well as extract parameters that characterize charge transport in pristine organic films and organic D/A composites from transient photocurrents. In pristine ADT-TES-F films, simulations revealed two competing charge photogeneration pathways: fast charge generation, on a ps or sub-ps time scale, with efficiencies below 10%, and slow, on the time scale of tens of nanoseconds, with efficiencies of about 11%–12%, at the applied electric fields of 40–80 kV/cm. The relative contribution of these pathways to the photocurrent was electric field dependent, with the contribution of the fast process increasing with applied electric field. However, the total charge photogeneration efficiency was weakly electric field dependent exhibiting values of 14%–20% of the absorbed photon density. The remaining 80%–86% of the photoexcitation did not contribute to charge carrier generation at these time scales. In ADT-TES-F-based D/A composites, an additional pathway of charge photogeneration that proceeds via CT exciton dissociation contributed to the total charge photogeneration. In the composite with the 2 wt.% Pn-TIPS-F8 acceptor, which exhibits strong exciplex emission from a tightly bound D/A CT exciton, the contribution of the CT state to charge generation was small, ∼8%–12% of the total number of photogenerated charge carriers, dependent on the electric field. In contrast, in the composite with 2 wt.% PCBM acceptor, the CT state contributed about a half of all photogenerated charge carriers. In both D/A composites, the charge carrier mobilities were reduced and trap densities and average trap depths were increased, as compared to a pristine ADT-TES-F donor film. A considerably slower recombination of free holes with trapped electrons was found in the composite with the PCBM acceptor, which led to slower decays of the transient photocurrent and considerably higher charge retention, as compared to a pristine ADT-TES-F donor film and the composite with the Pn-TIPS-F8 acceptor.

[1]A. J. Heeger, Chem. Soc. Rev. **39**, 2354 (2010).
[2]I. D. W. Samuel and G. A. Turnbull, Chem. Rev. **107**, 1272 (2007).
[3]Y. Kim, M. Ballarotto, D. Park, M. Du, W. Cao, C. H. Lee, W. N. Herman, and D. B. Romero, Appl. Phys. Lett. **91**, 193510 (2007).
[4]S. Moller, S. Forrest, C. Perlov, W. Jackson, and C. Taussig, J. Appl. Phys. **94**, 7811 (2003).
[5]O. Ostroverkhova and W. E. Moerner, Chem. Rev. **104**, 3267 (2004).
[6]B. Walker, C. Kim, and T.-Q. Nguyen, Chem. Mater. **23**, 470 (2011).
[7]Y. Sun, G. C. Welch, W. L. Leong, C. J. Takacs, G. C. Bazan, and A. J. Heeger, Nature Mater. **11**, 44 (2012).
[8]A. Mishra and P. Bäuerle, Ang. Chem. **124**, 2060 (2012).
[9]A. A. Bakulin, A. Rao, V. G. Pavelyev, P. H. M. van Loosdrecht, M. S. Pshenichnikov, D. Niedzialek, J. Cornil, D. Beljonne, and R. H. Friend, Science **335**, 1340 (2012).
[10]S. Singh, B. Pandit, T. P. Basel, S. Li, D. Laird, and Z. V. Vardeny, Phys. Rev. B **85**, 205206 (2012).
[11]G. Sliaužys, K. Arlauskas, and V. Gulbinas, Phys. Status Solidi A **209**, 1302 (2012).
[12]P. E. Schwenn, K. Gui, Y. Zhang, P. L. Burn, P. Meredith, and B. J. Powell, Org. Electron. **13**, 2538 (2012).
[13]G. Grancini, M. Maiuri, D. Fazzi, A. Petrozza, H.-J. Egelhaaf, D. Brida, G. Cerullo, and G. Lanzani, Nature Mater. **12**, 29 (2012).

[14]K. Aryanpour, D. Psiachos, and S. Mazumdar, Phys. Rev. B **81**, 085407 (2010).

[15]M. Mingebach, S. Walter, V. Dyakonov, and C. Deibel, Appl. Phys. Lett. **100**, 193302 (2012).

[16]R. D. Pensack and J. B. Asbury, Chem. Phys. Lett. **515**, 197 (2011).

[17]F. Etzold, I. A. Howard, R. Mauer, M. Meister, T.-D. Kim, K.-S. Lee, N. S. Baek, and F. Laquai, J. Am. Chem. Soc. **133**, 9469 (2011).

[18]M. A. Faist, T. Kirchartz, W. Gong, R. S. Ashraf, I. McCulloch, J. C. de Mello, N. J. Ekins-Daukes, D. D. C. Bradley, and J. Nelson, J. Am. Chem. Soc. **134**, 685 (2012).

[19]A. E. Jailaubekov, A. P. Willard, J. R. Tritsch, W.-L. Chan, N. Sai, R. Gearba, L. G. Kaake, K. J. Williams, K. Leung, P. J. Rossky, and X.-Y. Zhu, Nature Mater. **12**, 66 (2013).

[20]S. D. Dimitrov, A. A. Bakulin, C. B. Nielsen, B. C. Schroeder, J. Du, H. Bronstein, I. McCulloch, R. H. Friend, and J. R. Durrant, J. Am. Chem. Soc. **134**, 18189 (2012).

[21]A. A. Bakulin, S. D. Dimitrov, A. Rao, P. C. Y. Chow, C. B. Nielsen, B. C. Schroeder, I. McCulloch, H. J. Bakker, J. R. Durrant, and R. H. Friend, J. Phys. Chem. Lett **4**, 209 (2013).

[22]W. Zhang, Y.-W. Wang, R. Hu, L.-M. Fu, X.-C. Ai, J.-P. Zhang, and J.-H. Hou, J. Phys. Chem. C **117**, 735 (2013).

[23]G. Ren, C. W. Schlenker, E. Ahmed, S. Subramaniyan, S. Olthof, A. Kahn, D. S. Ginger, and S. A. Jenekhe, Adv. Funct. Mater. **23**, 1238 (2013).

[24]D. H. K. Murthy, M. Gao, M. J. W. Vermeulen, L. D. A. Siebbeles, and T. J. Savenije, J. Phys. Chem. C **116**, 9214 (2012).

[25]T. W. Holcombe, J. E. Norton, J. Rivnay, C. H. Woo, L. Goris, C. Piliego, G. Griffini, A. Sellinger, J.-L. Bredas, A. Salleo, and J. M. J. Frechet, J. Am. Chem. Soc. **133**, 12106 (2011).

[26]L. G. Kaake, J. J. Jasieniak, R. C. Bakus, G. C. Welch, D. Moses, G. C. Bazan, and A. J. Heeger, J. Am. Chem. Soc. **134**, 19828 (2012).

[27]M. J. Kendrick, A. Neunzert, M. M. Payne, B. Purushothaman, B. D. Rose, J. E. Anthony, M. M. Haley, and O. Ostroverkhova, J. Phys. Chem. C **116**, 18108 (2012).

[28]D. Credgington, F. C. Jamieson, B. Walker, T.-Q. Nguyen, and J. R. Durrant, Adv. Mater. **24**, 2135 (2012).

[29]R. Fitzner, C. Elschner, M. Weil, C. Uhrich, C. Koerner, M. Riede, K. Leo, M. Pfeiffer, E. Reinold, E. Mena-Osteritz, and P. Baeuerle, Adv. Mater. **24**, 675 (2012).

[30]Y. S. Chung, N. Shin, J. Kang, J. Jo, V. M. Prabhu, S. K. Satija, R. J. Kline, D. M. DeLongchamp, M. F. Toney, M. A. Loth, B. Purushothaman, J. E. Anthony, and D. Y. Yoon, J. Am. Chem. Soc. **133**, 412 (2011).

[31]Y.-F. Lim, Y. Shu, S. R. Parkin, J. E. Anthony, and G. G. Malliaras, J. Mater. Chem. **19**, 3049 (2009).

[32]S. K. Park, D. A. Mourey, S. Subramanian, J. E. Anthony, and T. N. Jackson, Appl. Phys. Lett. **93**, 043301 (2008).

[33]A. D. Platt, J. Day, S. Subramanian, J. E. Anthony, and O. Ostroverkhova, J. Phys. Chem. C **113**, 14006 (2009).

[34]S. K. Park, T. N. Jackson, J. E. Anthony, and D. A. Mourey, Appl. Phys. Lett. **91**, 063514 (2007).

[35]J. E. Anthony, Chem. Rev. **106**, 5028 (2006).

[36]H. van Eersel, R. A. J. Janssen, and M. Kemerink, Adv. Funct. Mater. **22**, 2700 (2012).

[37]M. C. Heiber and A. Dhinojwala, J. Chem. Phys. **137**, 014903 (2012).

[38]J. Nelson, Phys. Rev. B **67**, 155209 (2003).

[39]C. Soci, D. Moses, Q.-H. Xu, and A. Heeger, Phys. Rev. B **72**, 245204 (2005).

[40]L. Kulikovsky, D. Neher, E. Mecher, K. Meerholz, H.-H. Hörhold, and O. Ostroverkhova, Phys. Rev. B **69**, 125216 (2004).

[41]O. Ostroverkhova and K. D. Singer, J. Appl. Phys. **92**, 1727 (2002).

[42]I. Hwang, C. R. McNeill, and N. C. Greenham, J. Appl. Phys. **106**, 094506 (2009).

[43]J.-T. Shieh, C.-H. Liu, H.-F. Meng, S.-R. Tseng, Y.-C. Chao, and S.-F. Horng, J. Appl. Phys. **107**, 084503 (2010).

[44]L. Koster, E. Smits, V. Mihailetchi, and P. Blom, Phys. Rev. B **72**, 085205 (2005).

[45]T. Kirchartz, B. E. Pieters, K. Taretto, and U. Rau, Phys. Rev. B **80**, 035334 (2009).

[46]A. Petersen, A. Ojala, T. Kirchartz, T. Wagner, F. Würthner, and U. Rau, Phys. Rev. B **85**, 245208 (2012).

[47]W. E. B. Shepherd, A. D. Platt, M. J. Kendrick, M. A. Loth, J. E. Anthony, and O. Ostroverkhova, J. Phys. Chem. Lett. **2**, 362 (2011).

[48]W. E. B. Shepherd, A. D. Platt, D. Hofer, O. Ostroverkhova, M. Loth, and J. E. Anthony, Appl. Phys. Lett. **97**, 163303 (2010).

[49]Y. Shang, Q. Li, L. Meng, D. Wang, and Z. Shuai, Theor. Chem. Acc. **129**, 291 (2011).

[50]K. Maturova, M. Kemerink, M. M. Wienk, D. S. H. Charrier, and R. A. J. Janssen, Adv. Funct. Mater. **19**, 1379 (2009).

[51]C. Deibel, A. Wagenpfahl, and V. Dyakonov, Phys. Status Solidi (RRL) **2**, 175 (2008).

[52]E. Knapp, R. Häusermann, H. U. Schwarzenbach, and B. Ruhstaller, J. Appl. Phys. **108**, 054504 (2010).

[53]W. Tress, K. Leo, and M. Riede, Phys. Rev. B **85**, 155201 (2012).

[54]J. Day, S. Subramanian, J. E. Anthony, Z. Lu, R. J. Twieg, and O. Ostroverkhova, J. Appl. Phys. **103**, 123715 (2008).

[55]J. Day, A. D. Platt, S. Subramanian, J. E. Anthony, and O. Ostroverkhova, J. Appl. Phys. **105**, 103703 (2009).

[56]V. Arkhipov, E. Emelianova, and H. Bässler, Phys. Rev. Lett. **82**, 1321 (1999).

[57]J. D. Servaites, B. M. Savoie, J. B. Brink, T. J. Marks, and M. A. Ratner, Energy Environ. Sci. **5**, 8343 (2012).

[58]A. Platt, M. Kendrick, M. Loth, J. Anthony, and O. Ostroverkhova, Phys. Rev. B **84**, 235209 (2011).

[59]C. Braun, J. Chem. Phys. **80**, 4157 (1984).

[60]K. Falkowski, W. Stampor, P. Grygiel, and W. Tomaszewicz, Chem. Phys. **392**, 122 (2012).

[61]V. I. Arkhipov and H. Bässler, in *Physics of Organic Semiconductors*, edited by W. Brütting (Wiley-VCH Verlag GmbH & Co. KGaA, 2005).

[62]J. Kalinowski, W. Stampor, and P. G. Di Marco, J. Chem. Phys. **96**, 4136 (1992).

[63]D. Wehenkel, L. Koster, M. Wienk, and R. Janssen, Phys. Rev. B **85**, 125203 (2012).

[64]G. Malliaras and J. Scott, J. Appl. Phys. **83**, 5399 (1998).

[65]See supplementary material at http://dx.doi.org/10.1063/1.4820259 for details of the fitting process, the calculation of initial conditions, exciton time-resolved dynamics, and simulated dependence of the photocurrent dynamics on trap-assisted recombination.

[66]S. Lacic and O. Inganäs, J. Appl. Phys. **97**, 124901 (2005).

[67]J. Scott and G. Malliaras, Chem. Phys. Lett. **299**, 115 (1999).

[68]S. G. Johnson, The NLOPT non-linear optimization package, version 2.3, 2012, see www.ab-initio.mit.edu/nlopt.

[69]T. Runarsson and X. Yao, IEEE Trans. Syst. Man. Cybern., Part C Appl. Rev. **35**, 233 (2005).

[70]M. J. D. Powell, *in Advances in Optimization and Numerical Analysis*, edited by S. Gomex and J.-P. Hennart (Kluwer Academic, Dordrecht, 1994), p. 51.

[71]D. J. Gundlach, J. E. Royer, S. K. Park, S. Subramanian, O. D. Jurchescu, B. H. Hamadani, A. J. Moad, R. J. Kline, L. C. Teague, O. Kirillov, C. A. Richter, J. G. Kushmerick, L. J. Richter, S. R. Parkin, T. N. Jackson, and J. E. Anthony, Nature Mater. **7**, 216 (2008).

[72]S. Gorgolis, A. Giannopoulou, and P. Kounavis, J. Appl. Phys. **113**, 123102 (2013).

[73]O. Kwon, V. Coropceanu, N. E. Gruhn, J. C. Durivage, J. G. Laquindanum, H. E. Katz, J. Cornil, and J. L. Bredas, J. Chem. Phys. **120**, 8186 (2004).

[74]C. K. Renshaw, J. D. Zimmerman, B. E. Lassiter, and S. R. Forrest, Phys. Rev. B **86**, 085324 (2012).

[75]J. Kniepert, M. Schubert, J. C. Blakesley, and D. Neher, J. Phys. Chem. Lett. **2**, 700 (2011).

[76]F. C. Jamieson, T. Agostinelli, H. Azimi, J. Nelson, and J. R. Durrant, J. Phys. Chem. Lett. **1**, 3306 (2010).

[77]P. Miranda, D. Moses, and A. Heeger, Phys. Rev. B **64**, 081201 (2001).

[78]O. Ostroverkhova, D. Cooke, S. Shcherbyna, R. Egerton, F. Hegmann, R. Tykwinski, and J. Anthony, Phys. Rev. B **71**, 035204 (2005).

[79]O. Ostroverkhova, D. G. Cooke, F. A. Hegmann, R. R. Tykwinski, S. R. Parkin, and J. E. Anthony, Appl. Phys. Lett. **89**, 192113 (2006).

[80]H. Liang, W. Cao, M. Du, Y. Kim, W. Herman, and C. Lee, Chem. Phys. Lett. **419**, 292 (2006).

[81]D. Moses, C. Soci, X. Chi, and A. Ramirez, Phys. Rev. Lett. **97**, 067401 (2006).

[82]J. Day, A. D. Platt, O. Ostroverkhova, S. Subramanian, and J. E. Anthony, Appl. Phys. Lett. **94**, 013306 (2009).

[83]J.-F. Glowe, M. Perrin, D. Beljonne, S. C. Hayes, F. Gardebien, and C. Silva, Phys. Rev. B **81**, 041201 (2010).

[84]O. Ostroverkhova, *in Organic Electronics: Emerging Concepts and Technologies*, edited by F. Cicoira and C. Santato (Wiley-VCH, 2013).